Chapter 3
Identifying Coupling Directions by Recurrences

Yong Zou, M. Carmen Romano, Marco Thiel, and Jürgen Kurths

Abstract The identification of the coupling direction from measured time series taking place in a group of interacting components is an important challenge for many experimental studies. In *Part I* of this chapter, we introduce a method to detect and quantify the asymmetry of the coupling between two interacting systems based on their recurrence properties. This method can detect the direction of the coupling in weakly as well as strongly coupled systems. It even allows detecting the asymmetry

Y. Zou (✉)
Department of Physics, East China Normal University, Shanghai 200062, China

Potsdam Institute for Climate Impact Research, P.O. Box 601203, 14412 Potsdam, Germany
e-mail: yzou@phy.ecnu.edu.cn

M.C. Romano • M. Thiel
Institute for Complex Systems and Mathematical Biology, University of Aberdeen, Aberdeen AB243UE, UK

J. Kurths
Potsdam Institute for Climate Impact Research, P.O. Box 601203, 14412 Potsdam, Germany

Department of Physics, Humboldt University Berlin, Newtonstr. 15, 12489 Berlin, Germany

Institute for Complex Systems and Mathematical Biology, University of Aberdeen, Aberdeen AB243UE, UK

C.L. Webber, Jr. and N. Marwan (eds.), *Recurrence Quantification Analysis*, Understanding Complex Systems, DOI 10.1007/978-3-319-07155-8_3,

of the coupling in the more challenging case of structurally different systems and it is very robust against noise. We also address the problem of detecting the asymmetry of the coupling in passive experiments, i.e., when the strength of the coupling cannot be systematically changed, which is of great relevance for the analysis of experimental time series. *Part II* of this chapter hinges on a generalisation of conditional probability of recurrence to the case of multivariate time series where indirect interactions might be present. We test our method by an example of three coupled Lorenz systems. Our results confirm that the proposed method has much potential to identify indirect coupling.

3.1 Part I: Estimation of the Direction of the Coupling by Conditional Probabilities of Recurrence

3.1.1 Introduction: Part I

The interplay among different complex dynamical systems is a central issue in nonlinear dynamics as well as in nonlinear time series analysis. Under certain assumptions different types of synchronisation can occur between the interacting systems. This topic has been intensively studied in the last years and has been applied to various fields, such as physics, engineering and biology [2, 6, 8, 9, 29, 52, 53, 55]. In such systems it is important not only to analyse the synchronisation but also to identify causal (drive-response) or mutual relationships. There are four major approaches to address this problem: state-space based methods [4, 31, 32, 42], information theory based methods [26, 41, 54], methods based on the interrelations between the phases of the systems under consideration [37, 38], and recurrence-based methods [12, 13, 18, 24, 33].

In the state-space based approach, the state vectors are usually reconstructed by means of delay embedding [19]. The direction of the coupling is then assessed by considering the correspondence between neighbours in the phase spaces of the driver and response. If there exists a functional relationship between the driver X and the response system Y, i.e., $\mathbf{y}(t) = \Psi(\mathbf{x}(t))$, they are said to be generalised synchronised [20, 39]. If Ψ exists and is smooth, it follows that close states of the driver will be mapped to close states of the response. However, if Ψ is bijective, also close states of the response will be mapped to close states of the driver. Therefore, if X and Y are generalised synchronised it is in general impossible to assess the direction of the coupling reliably and the state-space based methods are only applicable in the non-synchronised regime [25, 43].

The understanding of a driver-response relationship was firstly evaluated in a linear framework by bivariate autoregressive models, by means of Granger causality [16]. This has been mainly applied to economy and neurosciences [7]. From the nonlinear perspective, there are several methods based on information theory to determine the direction of the coupling [5, 14, 26, 41, 47]. They are usually applied to systems which are strongly coupled. In order to treat also weakly coupled

systems, the phases of the signals are determined beforehand, and then information theory based indices are applied to the phases [27,28]. In [38], a technique based on the fitting of the functional relationship between the phases of the two interacting systems has been proposed to detect and quantify the asymmetry in the coupling. A systematic comparison between the phase-dynamics and the state-space approach in the case of weak directional coupling has been done in [43], where the authors concluded that neither one of the approaches is generally superior and that both approaches have difficulties in assessing the direction of the coupling in systems which are structurally different.

In Part *I* of this chapter, we summarize the recently proposed method to uncover directional coupling. This approach is based on the recurrence properties of both interacting systems. The concept of recurrence has been used to detect relationships between interacting systems in [46], where the so-called synchronisation likelihood has been introduced. This method allows for a multivariate analysis of generalised synchronisation. Moreover, in [34] the concept of recurrence has been used to quantify a weaker form of synchronisation, namely phase synchronisation. Here, we extend these measures in order to detect the direction of the coupling. The proposed method is rather straightforward to compute, in contrast to the more complicated information theory approaches. Furthermore, it has the advantage that it is applicable to both weak and strong directional coupling, as well as to structurally different systems.

The outline of Part *I* of this chapter is as follows: in Sect. 3.1.2 we introduce measures for the analysis of directional coupling based on recurrences. In Sect. 3.1.3 we demonstrate the proposed measures in some numerical examples and discuss the choice of the parameters of the method in Sect. 3.1.4. In Sect. 3.1.5 we discuss the dependence of these measures on observational noise. We consider in Sect. 3.1.6 the problem of passive experiments, where the coupling strength between the two interacting systems cannot be varied systematically. In Sect. 3.1.7 we compare the proposed method with other existing techniques and, finally, we give some conclusions.

3.1.2 Detection of the Coupling Direction by Recurrences

Recurrence is a fundamental property of dynamical systems. The concept of recurrence was introduced by Poincaré [30], where he showed that the trajectory of a dynamical system with a measure preserving flow recurs infinitely many times to some neighbourhood of a former visited state on an invariant set in phase space. There are many different techniques in nonlinear dynamics which exploit the concept of recurrence [1, 15, 40]. We concentrate on the method of Recurrence Plots (RPs), introduced by Eckmann et al. to visualise the behaviour of dynamical systems in the phase space [10]. They are defined by means of the recurrence matrix

$$R^X_{i,j} = \Theta\left(\varepsilon - ||\mathbf{x}_i - \mathbf{x}_j||\right), \qquad i, j = 1, \ldots, N, \tag{3.1}$$

where $\mathbf{x}_i$ denotes the state of the system X at time $i\,\Delta t$ with Δt being the sampling rate, ε is a predefined threshold, $\Theta(\cdot)$ is the Heaviside function and N is the length of the trajectory considered. The RP is obtained plotting a dot at the coordinates (i, j) if $R_{i,j} = 1$. By looking at the patterns of the RP, one gets at the outset a visual impression about the dynamics of the system under consideration. In order to go beyond the visual impression, several measures have been proposed to quantify the patterns in the RP. They have found numerous applications in very different kinds of systems [21, 22]. Moreover, somehow more formal relationships between the patterns obtained in RPs and main dynamical invariants, such as K_2 and D_2, have been found [11, 51] (cf. Chap. 2). It has also been shown that the RP contains all necessary information to reconstruct the underlying trajectory, at least topologically [49].

The method of RPs has been extended to Joint Recurrence Plots (JRPs) to analyse the interplay of two or more dynamical systems [36, 46]. The JRP of X and Y is defined as

$$J_{R_{i,j}}^{X,Y} = \Theta\left(\varepsilon_X - ||\mathbf{x}_i - \mathbf{x}_j||\right) \Theta\left(\varepsilon_Y - ||\mathbf{y}_i - \mathbf{y}_j||\right), \tag{3.2}$$

i.e., a joint recurrence occurs if the system X recurs in its own phase space and simultaneously, the system Y recurs also in its own phase space. Based on JRPs it is possible to analyse different kinds of synchronisation of coupled complex systems [34, 45, 46]. In order to illustrate this, we consider two rather different chaotic oscillators, namely the Rössler system

$$\begin{aligned} \dot{x}_1 &= 2 + x_1(x_2 - 4), \\ \dot{x}_2 &= -x_1 - x_3, \\ \dot{x}_3 &= x_2 + 0.45x_3, \end{aligned} \tag{3.3}$$

which drives the Lorenz system

$$\begin{aligned} \dot{y}_1 &= -10(y_1 - y_2), \\ \dot{y}_2 &= 28u - y_2 - uy_3, \\ \dot{y}_3 &= uy_2 - 8/3y_3, \end{aligned} \tag{3.4}$$

by means of the variable $u = x_1 + x_2 + x_3$. In [20] it has been shown that the driven Lorenz system is asymptotically stable and that both systems are in generalised synchronisation. Hence, two close neighbours in the phase space of the driver system correspond to two close neighbours in the phase space of the driven system [39]. This relationship is reflected very clearly in the RPs of both systems. In Fig. 3.1a, c we plot the trajectories in phase space of the Rössler Eq. (3.3) and of the Lorenz system Eq. (3.4), respectively. To calculate their corresponding RPs, we have used the third component of each system and reconstructed the respective trajectories in phase space using delay embedding [19] with embedding dimension

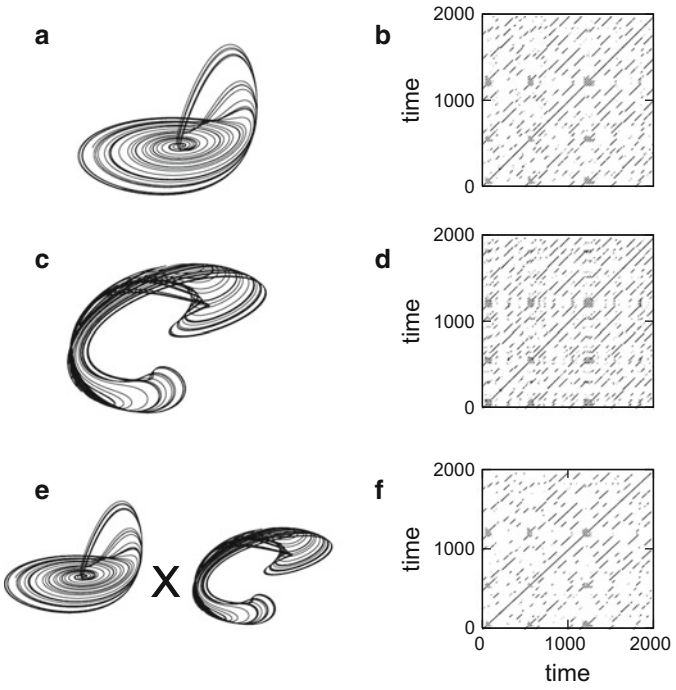

Fig. 3.1 (**a**) Rössler driving system, (**b**) the RP of the Rössler system ($m = 3, \tau = 5$), (**c**) the driven Lorenz system, (**d**) the RP of the Lorenz system ($m = 7, \tau = 5$), (**e**) representation of the "joint" system, and (**f**) the joint recurrence plot of both systems. The threshold for the computation of the RPs has been chosen so that the recurrence rate (number of recurrence points divided by N^2) is equal for both systems. In this case the recurrence rate was 0.005. The equations were integrated using fourth order Runge–Kutta of and the sampling time was 0.2

$m = 7$ and time delay $\tau = 5$ (the time step between two consecutive points being 0.2), since dealing with experimental time series, usually only one observable of the system is available. Even though the shapes of both attractors in the phase space look rather different (Fig. 3.1a, c), both RPs are very similar (Fig. 3.1b, d). Therefore, the joint recurrence plot (Fig. 3.1f) resembles the very similar recurrence patterns as the RPs of the single systems.

This property of joint recurrence plots has been treated in detail in [34], where it has been used for the detection of generalised synchronisation, also in more difficult cases where other methods, such as the mutual false nearest neighbours, are not appropriate any longer. In [46] the authors have introduced the synchronisation likelihood, which is a multivariate measure for generalised synchronisation. This measure is based on a very similar concept to the joint recurrence matrix of Eq. (3.2). However, the thresholds ε_X and ε_Y are not fixed for the whole trajectories, but are dependent on time.

Only considering the concept of joint recurrence is not sufficient to identify which system is the driver and which one is the response. In order to accomplish that, it is necessary to assess conditional probabilities of recurrence. Therefore, we propose the mean conditional probabilities of recurrence (MCR) between two systems X and Y, which are defined as follows

$$M_{CR}(Y|X) = \frac{1}{N}\sum_{i=1}^{N} p(\mathbf{y}_i|\mathbf{x}_i) = \frac{1}{N}\sum_{i=1}^{N} \frac{\sum_{j=1}^{N} J_{R_{i,j}}^{X,Y}}{\sum_{j=1}^{N} R_{i,j}^{X}}, \tag{3.5}$$

and

$$M_{CR}(X|Y) = \frac{1}{N}\sum_{i=1}^{N} p(\mathbf{x}_i|\mathbf{y}_i) = \frac{1}{N}\sum_{i=1}^{N} \frac{\sum_{j=1}^{N} J_{R_{i,j}}^{X,Y}}{\sum_{j=1}^{N} R_{i,j}^{Y}}, \tag{3.6}$$

where $p(\mathbf{y}_i|\mathbf{x}_i)$ is an estimate of the probability that the trajectory of Y recurs to the neighbourhood of $\mathbf{y}_i$ under the condition that the trajectory of X recurs to the neighbourhood of $\mathbf{x}_i$ ($p(\mathbf{x}_i|\mathbf{y}_i)$ is defined analogously). One can consider these measures as an extension of the methods presented in [34, 46].

The criterion that we use for detecting the asymmetry of the coupling is the following

$$\text{If } X \text{ drives } Y, \qquad M_{CR}(Y|X) < M_{CR}(X|Y). \tag{3.7a}$$

$$\text{If } Y \text{ drives } X, \qquad M_{CR}(X|Y) < M_{CR}(Y|X). \tag{3.7b}$$

If the coupling is symmetric, then $M_{CR}(X|Y) = M_{CR}(Y|X)$.

This criterion might appear counterintuitive at first, because if X is the driver, one could think that the probability of recurrence of a state $\mathbf{y}_i$ given that the state $\mathbf{x}_i$ recurs is larger than vice versa, since X is independent of Y.

A heuristic argumentation for this criterion is the following: if X drives Y, the dimension of Y will be in general larger than the dimension of X, because the evolution of Y is determined by both the states of X and Y. Moreover, the higher the complexity of Y, the smaller is the probability of recurrence of $\mathbf{y}_i \quad \forall i$. Hence, by increasing the coupling strength from X to Y, the probability $p(\mathbf{y}_i)$ that the trajectory of Y recurs to the neighbourhood of $\mathbf{y}_i$ will decrease. In contrast, the complexity of X remains constant with increasing coupling strength, because the evolution of X depends only on the states of X. Hence, the probability $p(\mathbf{x}_i)$ that the trajectory of X recurs to the neighbourhood of $\mathbf{x}_i$ does not change with the coupling strength. We choose the thresholds ε_X and ε_Y in such a way, that if the coupling strength is equal to zero, $\langle p(\mathbf{x}_i)\rangle = \langle p(\mathbf{y}_i)\rangle$. Therefore, if the coupling strength from X to Y is larger than zero, in general $p(\mathbf{y}_i) < p(\mathbf{x}_i)$. That implies $p(\mathbf{x}_i, \mathbf{y}_i)/p(\mathbf{x}_i) < p(\mathbf{x}_i, \mathbf{y}_i)/p(\mathbf{y}_i)$ and hence, $M_{CR}(Y|X) < M_{CR}(X|Y)$.

3.1.3 Numerical Examples

In this section we illustrate the performance of the proposed measures for the direction of the coupling by three kinds of examples: strongly coupled systems (close to the onset of complete synchronisation), weakly coupled systems (close to the onset of phase synchronisation), and structurally different systems. The number of data points of the trajectories used in each case, if not stated otherwise, is equal to 10,000 throughout the chapter.

3.1.3.1 Strongly Coupled Systems

We consider two unidirectionally coupled Hénon maps, given by the following equations

$$\begin{aligned} x_1(i+1) &= 1.4 - x_1(i)^2 + b_1 x_2(i), \\ x_2(i+1) &= x_1(i) \end{aligned} \tag{3.8}$$

for the driving system X, and

$$\begin{aligned} y_1(i+1) &= 1.4 - \left(\mu x_1(i) y_1(i) + (1-\mu) y_1^2(i)\right) + b_2 y_2(i), \\ y_2(i+1) &= y_1(i) \end{aligned} \tag{3.9}$$

for the response system Y [32], where μ is the coupling strength. We analyse both the case of identical systems ($b_1 = b_2 = 0.3$) and non-identical systems ($b_1 = 0.1$, $b_2 = 0.3$). To mimic this problem for data analysis, we assume that we have observed the two scalar time series $\{x_1(i)\}_{i=1}^N$ and $\{y_1(i)\}_{i=1}^N$. Hence, we have to reconstruct the trajectories of X and Y in phase space [19]; this will be done by delay embedding. We choose embedding dimension $m = 3$ and time delay $\tau = 1$, but we note that the results are qualitatively the same with other reasonable choices. The values of the thresholds ε_X and ε_Y have been chosen such that for no coupling both mean probabilities of recurrences $\langle p(\mathbf{x}(i)) \rangle$ and $\langle p(\mathbf{y}(i)) \rangle$ are equal to 0.01. We use 10,000 data points and compute the indices $M_{CR}(X|Y)$ and $M_{CR}(Y|X)$ in dependence on the coupling strength μ. The results are shown in Fig. 3.2.

For two identical Hénon maps (Fig. 3.2a), the onset to identical synchronisation occurs at approximately $\mu = 0.65$, as reported in [26,32]. As expected from this, we yield for $\mu > 0.65$, $M_{CR}(X|Y) = M_{CR}(X|Y)$. Before the onset of synchronisation, we get $M_{CR}(X|Y) > M_{CR}(Y|X)$, indicating correctly the direction of the coupling.

On the other hand, for the non-identical Hénon maps, the onset to generalised synchronisation occurs at approximately $\mu = 0.4$ [32]. Note that in general the detection of the directionality is only possible before the onset of synchronisation. In the case of identical synchronisation, the series $\{x_i\}$ and $\{y_i\}$ are identical and hence there is no possibility of establishing the causal relationship between X and Y just from the data. This argument can be also extended to the case

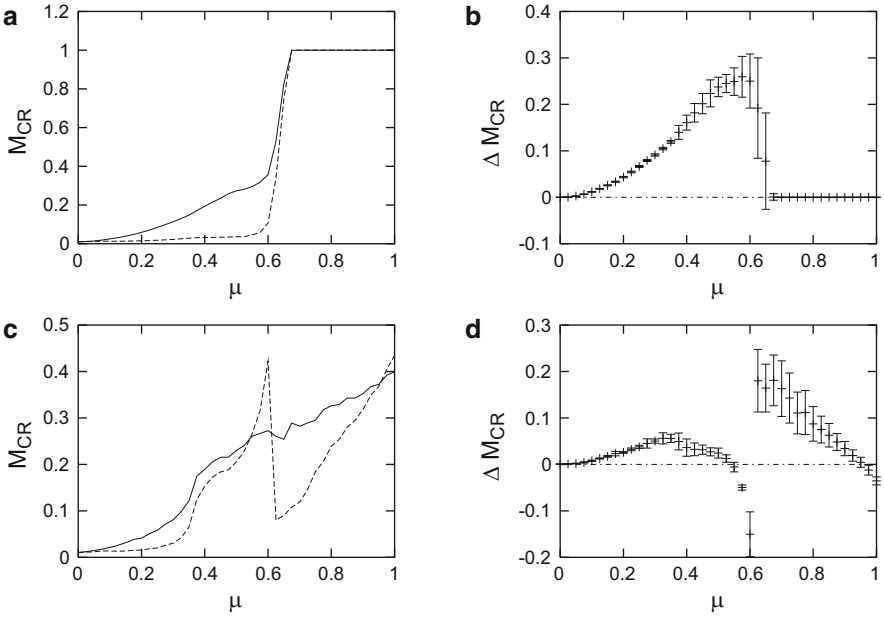

Fig. 3.2 Mean conditional probabilities of recurrence $M_{CR}(X|Y)$ (*solid*) and $M_{CR}(Y|X)$ (*dashed*) for two unidirectionally coupled identical (**a**) and non-identical (**c**) Hénon maps. The system X is in both cases the driver, and hence, $M_{CR}(X|Y) > M_{CR}(Y|X)$. For each value of the coupling strength μ, the mean value over 100 trajectories for uniformly distributed initial conditions has been computed. In **b and d** we have plotted the mean value of the difference $\Delta M_{CR} = M_{CR}(X|Y) - M_{CR}(Y|X)$ over 100 trajectories and the corresponding standard deviation for the identical and non-identical Hénon systems, respectively. The zero line is also plotted for orientation (*dotted-dashed*)

of generalised synchronisation, where the systems are related by a one-to-one function [4]. Therefore, in the case of the two non-identical Hénon maps the directionality parameters are reliable for $0 < \mu < 0.4$. The sharp drop of $M_{CR}(Y|X)$ (dashed curve in Fig. 3.2c) at approximately $\mu = 0.6$ is due to the non-monotonic dependence of the maximum Lyapunov exponent of the response system on the coupling strength [32].

3.1.3.2 Weakly Coupled Systems

Now we study two non-identical unidirectionally coupled Lorenz systems, given by the equations

$$\begin{aligned} \dot{x}_1 &= 10(x_1 - x_2), \\ \dot{x}_2 &= 40x_1 - x_2 - x_1x_3, \\ \dot{x}_3 &= x_1x_2 - 8/3x_3, \end{aligned} \tag{3.10}$$

for the driver system X and

$$\begin{aligned}\dot{y}_1 &= 10(y_2 - y_1) + \mu(x_1 - y_1),\\ \dot{y}_2 &= 35y_1 - y_2 - y_1 y_2,\\ \dot{y}_3 &= y_1 y_2 - 8/3 y_3,\end{aligned} \tag{3.11}$$

for the response system Y. The equations have been integrated by a fourth-order Runge–Kutta algorithm and the time step between two consecutive points is equal to 0.03. We use 10,000 data points and assume that only the scalar variables x_3 and y_3 have been observed. The embedding parameters used for the reconstruction are $m = 10$ and $\tau = 12$. As in the former case, the results do not depend on the details of this choice. We have not used the optimal embedding parameters which can be estimated by, e.g., the methods of false nearest neighbours and the autocorrelation function, in order to show that the results are robust with respect to different embedding parameters [43]. We compute the directionality parameters MCR in dependence on the coupling strength μ between 0 and 10, which is before the onset of phase synchronisation [43]. The results are shown in Fig. 3.3a. We clearly see that $M_{CR}(X|Y) > M_{CR}(Y|X)$ for all computed values of the coupling strength μ, i.e., the recurrence based indices detect the direction of the coupling correctly. The values of the thresholds ε_X and ε_Y have been chosen such that for no coupling both mean probabilities of recurrences $\langle p(\mathbf{x}(i))\rangle$ and $\langle p(\mathbf{y}(i))\rangle$ are equal to 0.01. However, note that for $\mu = 0$, the values of $M_{CR}(X|Y)$ and $M_{CR}(Y|X)$ are larger and not equal to 0.01, as one would expect. This is because the estimated joint probability of recurrence is larger than $(0.01)^2$, due to the limited number of data used for the computation. Nevertheless, the expected qualitative behaviour, i.e. $M_{CR}(X|Y) > M_{CR}(Y|X)$ still holds, which is the important fact for our analysis.

The next example that we consider is a bidirectionally coupled system, namely, two stochastic Van der Pol oscillators with slightly different mean frequencies ω_x and ω_y

$$\begin{aligned}\ddot{x} &= 0.2(1 - x^2)\dot{x} - \omega_x^2 x + \xi_x + 0.03(y - x),\\ \ddot{y} &= 0.2(1 - y^2)\dot{y} - \omega_y^2 y + \xi_y + \mu(x - y),\end{aligned} \tag{3.12}$$

where $\omega_x = 1.02$ and $\omega_y = 0.98$, ξ_x and ξ_y are independent Gaussian white noise with standard deviation 0.04. This example has been considered in [38, 43]. The equations have been integrated with the Euler scheme and the sampling time was 0.1π. The variables x and y have been used to reconstruct the phase space with embedding dimension 10 and delay 12, as in the former case. The thresholds ε_X and ε_Y have been chosen such that for symmetrical coupling $\langle p(\mathbf{x}_i)\rangle = \langle p(\mathbf{y}_i)\rangle = 0.1$. The results for the indices MCR are shown in Fig. 3.3b in dependence on the coupling strength μ. For $\mu < 0.03$, $M_{CR}(X|Y) < M_{CR}(Y|X)$, since the coupling is stronger from Y to X than vice versa. At the coupling strength 0.03, we obtain $M_{CR}(X|Y) = M_{CR}(Y|X)$, because the coupling is symmetrical, and for $\mu > 0.03$,

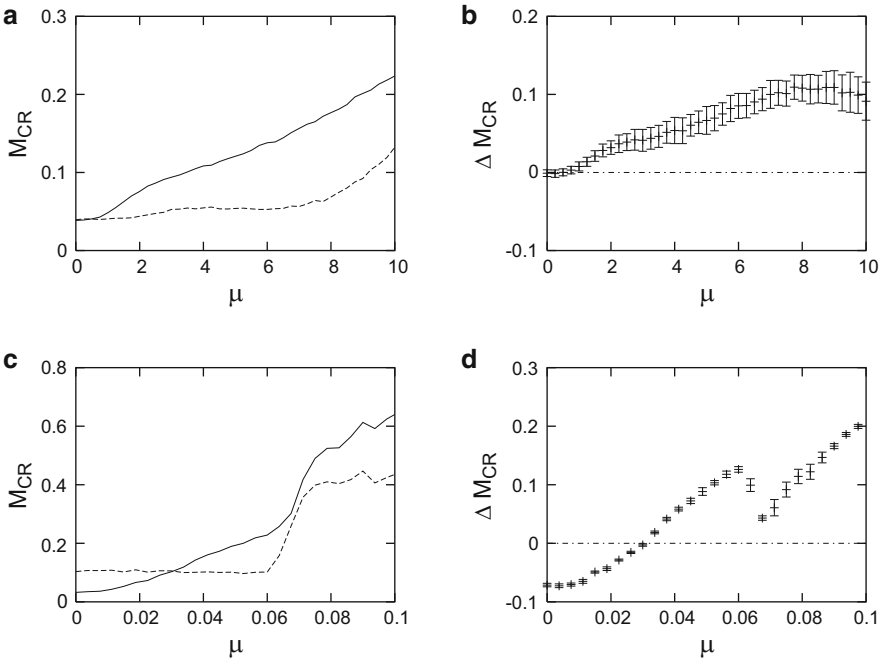

Fig. 3.3 Mean conditional probabilities of recurrence $M_{CR}(X|Y)$ (*solid*) and $M_{CR}(Y|X)$ (*dashed*) for (**a**): two weakly unidirectionally coupled non-identical Lorenz systems. For each value of the coupling strength μ, the mean value over 100 trajectories for uniformly distributed initial conditions has been computed. The system X is the driver, and hence, $M_{CR}(X|Y) > M_{CR}(Y|X)$. (**c**): Two weakly bidirectionally coupled stochastic Van der Pol oscillators. The coupling strength from X to Y is fixed and equal to 0.3. In **b** and **d** we have plotted the mean value of $\Delta M_{CR} = M_{CR}(X|Y) - M_{CR}(Y|X)$ and the corresponding standard deviation over 100 trajectories for each system, respectively. The zero line is also plotted for orientation (*dotted-dashed*)

we observe that $M_{CR}(X|Y) > M_{CR}(Y|X)$, because the coupling from X to Y is stronger than vice versa. Note that at $\mu \approx 0.06$ both oscillators become phase synchronised and the value of $M_{CR}(Y|X)$ increases much faster.

3.1.3.3 Structurally Different Systems

Next, we study the more challenging case of two structurally different systems, namely a stochastic Van der Pol system which drives a Rössler system. The equation of the driving system X is

$$\ddot{x} = 0.1(1 - x^2)\dot{x} - \omega_x^2 x + \xi_x, \tag{3.13}$$

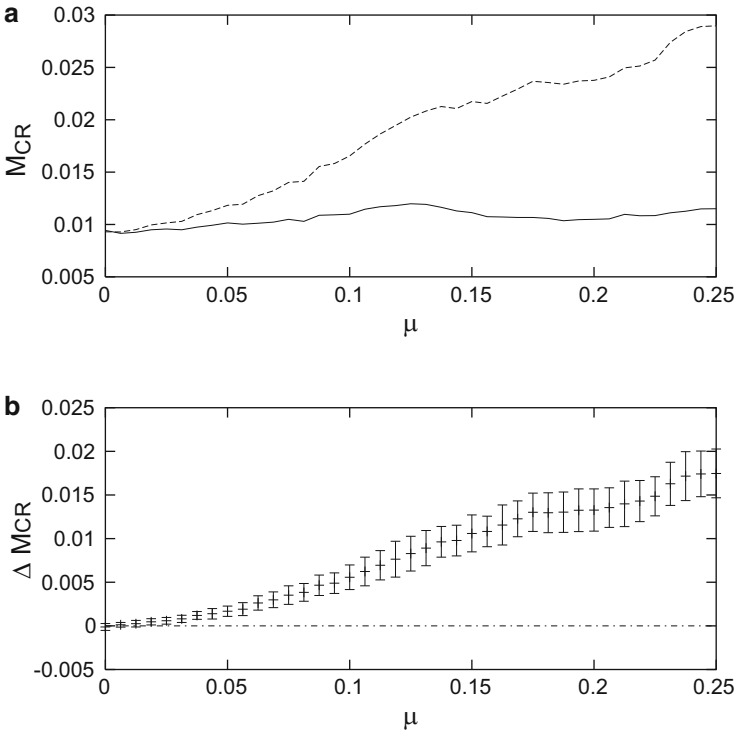

Fig. 3.4 (**a**) Mean conditional probabilities of recurrence $M_{CR}(X|Y)$ (*solid*) and $M_{CR}(Y|X)$ (*dashed*) for the chaotic Rössler system driven by the stochastic Van der Pol system. For each value of the coupling strength μ, the mean value over 100 trajectories for uniformly distributed initial conditions has been computed. The system X is the driver, and hence, we find $M_{CR}(X|Y) > M_{CR}(Y|X)$. (**b**) Mean value of the difference $\Delta M_{CR} = M_{CR}(X|Y) - M_{CR}(Y|X)$ and corresponding standard deviation over 100 trajectories. The zero line is also plotted for orientation (*dotted-dashed*)

where $\omega_x = 0.98$ and ξ_x is Gaussian white noise with standard deviation 0.05. The equations of the response system Y are given by

$$\begin{aligned} \dot{y}_1 &= -y_2 - y_3, \\ \dot{y}_2 &= y_1 + 0.15y_2 + \mu x, \\ \dot{y}_3 &= (y_1 - 10)y_3 + 0.2. \end{aligned} \tag{3.14}$$

The equations have been integrated with a Euler scheme and the sampling time was 0.1π. The phase space has been reconstructed using the variables x and y_1 and embedding dimension 10 and delay 12. The values of the thresholds ε_X and ε_Y have been chosen as in the former cases. The curves for MCR are shown in dependence on the coupling strength μ in Fig. 3.4. In this interval of values of the coupling

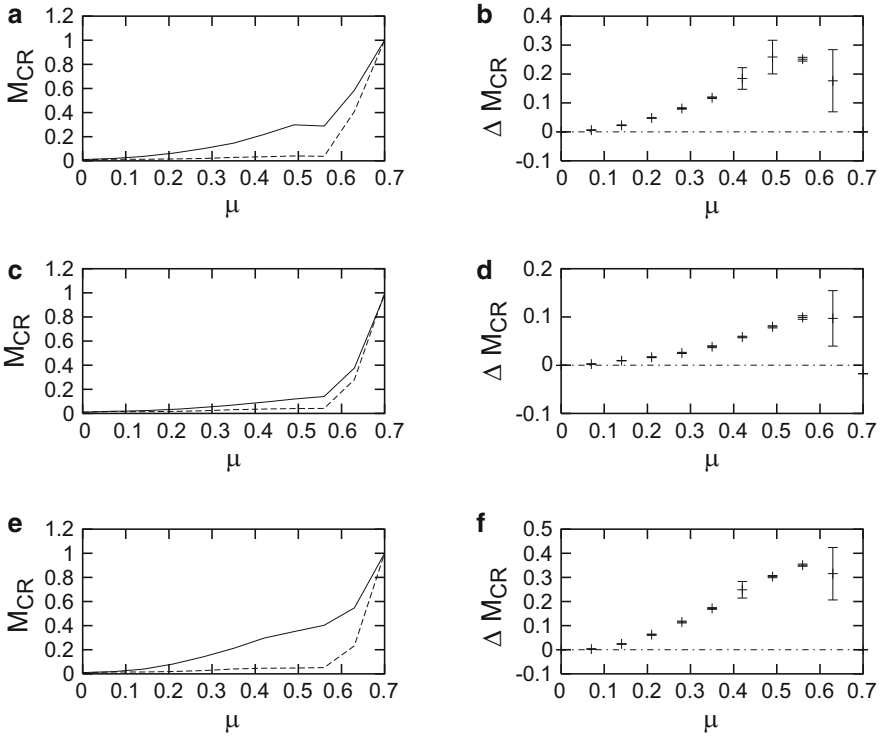

Fig. 3.5 Mean conditional probabilities of recurrence $M_{CR}(X|Y)$ (*solid*) and $M_{CR}(Y|X)$ (*dashed*) for two identical unidirectionally coupled Hénon maps for different choices of the embedding parameters: (**a**) $m = 3$, $\tau = 1$, (**c**) $m = 2$, $\tau = 3$,(**e**) $m = 5$, $\tau = 1$. For each value of the coupling strength μ, the mean value over ten trajectories for uniformly distributed initial conditions has been computed. In **b**, **d** and **f** the mean value and standard deviation over ten trajectories of the corresponding ΔM_{CR} are represented. The zero line is also plotted for orientation (*dotted-dashed*)

strength both systems are before the onset of phase synchronisation [43]. For all values of the coupling strength we obtain $M_{CR}(X|Y) > M_{CR}(Y|X)$, i.e., we are able to detect the direction of the coupling also in this case.

3.1.4 Choice of the Parameters

In order to compute the indices MCR, we need to fix four parameters: the embedding dimension m and the delay τ for the reconstruction of the phase space, and the thresholds ε_X and ε_Y for the computation of the recurrence matrices. As we have mentioned in the previous section, the special choice of the embedding parameters does not influence the results. In Fig. 3.5 we show the results for the

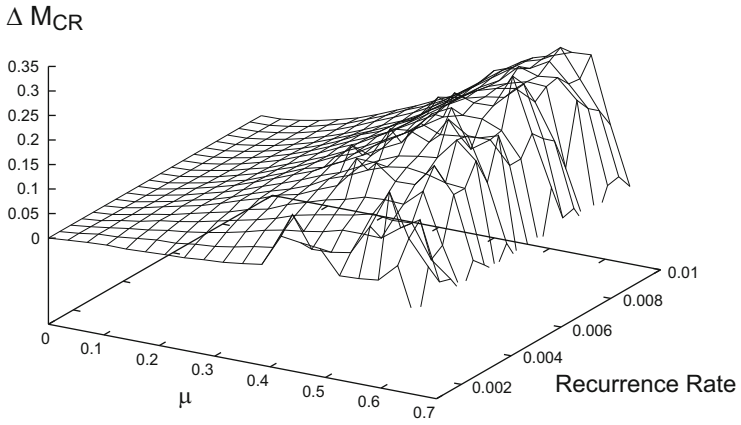

Fig. 3.6 $\Delta M_{CR} = M_{CR}(X|Y) - M_{CR}(Y|X)$ for two identical unidirectionally coupled Hénon maps in dependence on the coupling strength μ and the mean probability of recurrence or recurrence rate. For each value of the coupling strength μ, the mean value over ten trajectories for uniformly distributed initial conditions has been computed

direction parameters MCR for different choices of m and τ for the two identical unidirectionally coupled Hénon systems [Eqs. (3.8) and (3.9)]. We get, regardless of the choice of the embedding parameters, $M_{CR}(X|Y) > M_{CR}(Y|X)$ for all values of the coupling strength μ before the onset of synchronisation. This is the correct behaviour, since the system X is the driver and Y is the response.

With regard to the choice of the thresholds ε_X and ε_Y, we have mentioned in the previous section that they were chosen such that the mean probabilities of recurrence for both systems at coupling strength $\mu = 0$ are equal. In this way, it is not necessary to normalise the data x_i and y_i beforehand. In the numerical examples considered in Sect. 3.1.3, we chose the mean probability of recurrence to be equal to 0.01. In order to demonstrate how the results depend on this choice, we show in Fig. 3.6 $\Delta M_{CR} = M_{CR}(X|Y) - M_{CR}(Y|X)$ in dependence on the coupling strength and on the mean probability of recurrence (labelled as "Recurrence Rate" in the plot) for the Hénon systems [Eqs. (3.8) and (3.9)]. As system X is the driver, we expect that the surface ΔM_{CR} takes only positive values, which is the case in fact. Hence, we see that the estimation of MCR does not depend crucially on the choice of the thresholds ε_X and ε_Y. Hence, for a rather broad range of values of the thresholds, the direction of the coupling can be estimated correctly.

3.1.5 Influence of Noise

We now study the influence of observational noise on the MCR measures [Eqs. (3.5) and (3.6)]. Therefore, we add different levels of noise to the scalar time series

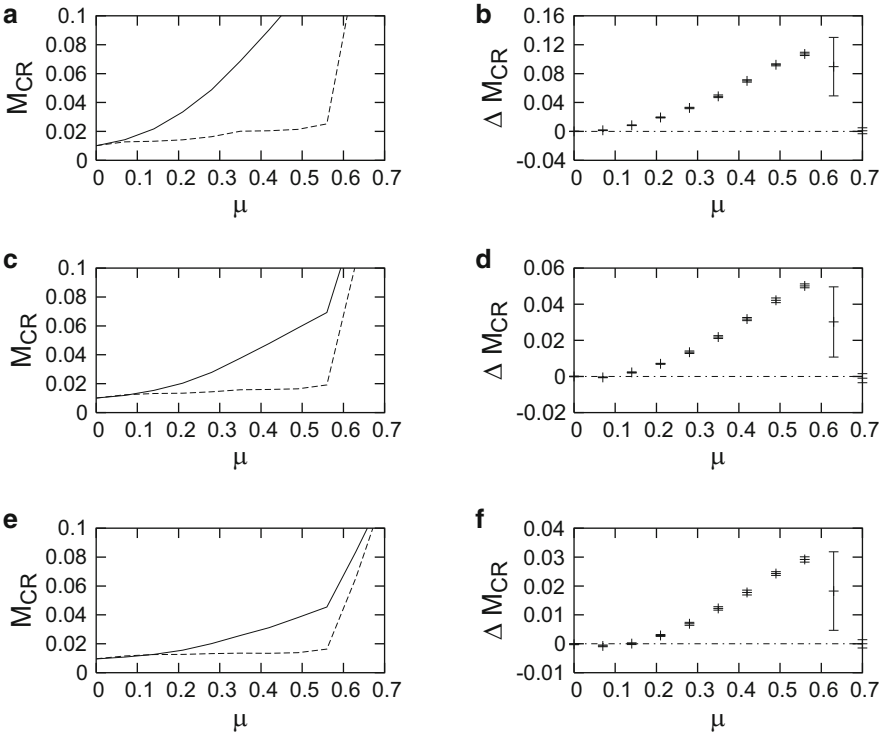

Fig. 3.7 $M_{CR}(X|Y)$ and $M_{CR}(Y|X)$ for two identical unidirectionally coupled Hénon maps contaminated by uniformly distributed noise in dependence on the coupling strength μ. (**a**) $\gamma = 0.2$, (**c**) $\gamma = 0.4$, (**e**) $\gamma = 0.6$. For each value of the coupling strength μ, the mean value over ten trajectories for uniformly distributed initial conditions has been computed. In **b**, **d** and (**f**) the corresponding mean value of the difference ΔM_{CR} and the standard deviation over ten trajectories are plotted. The zero line is also plotted for orientation (*dotted-dashed*)

$\{x_i\}_{i=1}^N$ and $\{y_i\}_{i=1}^N$, so that we compute the MCR indices for the series $x_i' = x_i + \gamma\sigma_x\eta_i^x$ and $y_i' = y_i + \gamma\sigma_y\eta_i^y$, where γ denotes the level of noise, σ_x and σ_y are the standard deviation of x_i and y_i, respectively, and η_x and η_y are two independent realisations of uniformly distributed random noise between -0.5 and 0.5. Figure 3.7 shows the results obtained for the MCR indices for three different values of γ corresponding to 20, 40 and 60 % of observational noise.

We observe that when the level of noise γ increases, it becomes more difficult to detect the asymmetry of the coupling for very small values of the coupling strength μ, because both curves $M_{CR}(X|Y)$ and $M_{CR}(Y|X)$ are almost equal. The larger the level of noise, the stronger must be the coupling strength in order to detect the asymmetry. Nevertheless, even with such high levels of observational noise, the asymmetry of the coupling can still be correctly detected for relatively small values of the coupling strength. Hence, we conclude that the MCR indices are a rather robust measure for the detection of the asymmetry of the coupling, also in the presence of relative high levels of observational noise.

3.1.6 Passive Experiments

One crucial problem of all measures for the detection of asymmetry of the coupling is the assessment of the significance of the results for passive experiments, i.e., when the coupling strength between both systems X and Y cannot be varied systematically in experiments. In such cases, we usually just have one scalar measurement sequence for each system $\{x_i\}_{i=1}^N$ and $\{y_i\}_{i=1}^N$ for a fixed coupling strength μ. This is the case in numerous situations. For example, the experimental data used in [23, 41] to illustrate the applicability of the method for the detection of the asymmetry of the coupling, are time series of breath rate and instantaneous heart rate of a sleeping human. It is very hard, if not impossible, to change the coupling strength between the respiratory and cardiological system of a person in a systematic way. The authors in [4] apply their proposed method for the detection of asymmetry of the coupling to intracranially recorded EEG data. In this case, it is also obvious that it is not possible to change the coupling strength between different areas of the brain, in a controlled manner.

In all these cases we obtain just one value for the directionality indices and then it is not trivial to decide whether the computed values have been obtained just by chance or whether they are significant. In order to address this question, we propose the following statistical test. Our null hypothesis is that the two systems X and Y are independent. To test this null hypothesis, we generate the so called *natural or twin surrogates* [50]. Suppose that we have one time series for each system $\{x_i\}_{i=1}^N$ and $\{y_i\}_{i=1}^N$ for a fixed coupling strength μ. The natural surrogates are trajectories from the same underlying dynamical systems X and Y with identical coupling strength μ between both of them, but starting at different initial conditions. We denote them by $\{x_i^s\}_{i=1}^N$ and $\{y_i^s\}_{i=1}^N$. If we have computed the directionality indices $M_{CR}(x|y)$ and $M_{CR}(y|x)$ for the measured time series, we can compare the obtained values with the distribution of $M_{CR}(x|y^s)$ and $M_{CR}(y^s|x)$,[1] respectively, generated from a large number of surrogates. If both systems X and Y are independent, the value $M_{CR}(x|y)$ will not differ significantly from the distribution of the values $M_{CR}(x|y^s)$. Otherwise, we can reject the null hypothesis, indicating that the obtained values for the directionality indices are significant.

At this point, the following question arises naturally: dealing with experimental data, one usually does not have a model for the governing dynamics. Then, how can one generate natural surrogates? The answer to this question has been addressed in [50], where an algorithm based on recurrence has been proposed to generate natural surrogates without knowing the underlying equations of the system. These recurrence based surrogates are called *twin surrogates* and have been applied in [50] to tackle the problem of passive experiments in phase synchronisation.

We now show the performance of the MCR method applying the twin surrogates test to analyse the estimation of the asymmetry of the coupling in [Eqs. (3.8)

[1] Note that considering $M_{CR}(x^s|y)$ and $M_{CR}(y|x^s)$ would yield the same result.

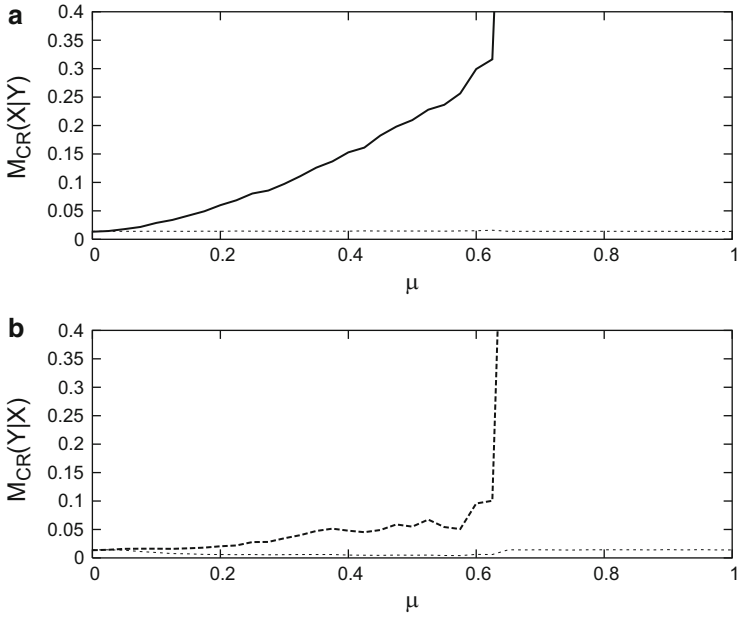

Fig. 3.8 (**a**) Mean conditional probability of recurrence $M_{CR}(X|Y)$ (*solid*) and 1 %-significance level (*dotted*) for two identical Hénon maps unidirectionally coupled. (**b**) $M_{CR}(Y|X)$ (*dashed*) and 1 %-significance level (*dotted*) for the same system. One hundred twin surrogates have been generated to estimate the significance level. The data have been normalised beforehand to have zero mean and standard deviation equal to one and $\varepsilon_X = \varepsilon_Y = 0.1$

and (3.9)]. We therefore generate 100 twin surrogates using the algorithm presented in [50]. We assume that we have scalar time series, and hence, use delay embedding to reconstruct the trajectory. We use embedding dimension $m = 3$ and delay $\tau = 1$, as in Sect. 3.1.3. The threshold for the generation of the surrogates is chosen to be $\delta = 0.09$ (see [50] for further details), according to the procedure given in [35]. Summarising, the following steps have to be undertaken for each value of the coupling strength μ:

- Choose the significance level α (i.e., $1-\alpha$ quantile of the distribution).
- Compute $M_{CR}(x|y)$ and $M_{CR}(y|x)$.
- Generate L twin surrogate time series $\{x_i^{s_j}\}_{i=1}^N$ and $\{y_i^{s_j}\}_{i=1}^N$, with $j = 1, \ldots, L$.
- Compute $M_{CR}(x|y^{s_j})$ and $M_{CR}(y^{s_j}|x)$ for $j = 1, \ldots, L$.
- Compute the α-significance value based on the distribution obtained in the former step.
- If $M_{CR}(x|y)$ and $M_{CR}(y|x)$ are larger than the corresponding α-significance values, reject the null hypothesis.

The results for [Eqs. (3.8) and (3.9)] are shown in Fig. 3.8.

The values of $M_{CR}(X|Y)$ and $M_{CR}(Y|X)$ are above the significance level in both cases for all values of the coupling strength. Hence, the null hypothesis is correctly rejected. Therefore, in the case that we have a passive experiment, this procedure can be applied to assess the significance of the results about the asymmetry of the coupling.

Note that in the case of passive experiments, we cannot apply the criterion proposed in Sect. 3.1.2 to choose the thresholds ε_X and ε_Y, such that for coupling strength equal to zero we have $\langle p(\mathbf{x}_i)\rangle = \langle p(\mathbf{y}_i)\rangle$, because we do not know the value of the coupling strength. Therefore, one has to apply another criterion to choose the thresholds ε_X and ε_Y. In the example shown in Fig. 3.8 we have normalised the data beforehand to have zero mean and standard deviation equal to one, and then we have chosen $\varepsilon_X = \varepsilon_Y = 0.1$. If both interacting systems are structurally similar, then $M_{CR}(X|Y)$ will be approximately equal to $M_{CR}(Y|X)$ for coupling strength equal to zero. However, if the interacting systems are structurally different, this approach might not hold anymore.

3.1.7 Comparison with Other Methods

As mentioned in the introduction, several methods have been proposed in the literature to estimate the direction of the coupling. Most of these methods can be divided in the following categories:

1. In order to apply the method introduced in [38], one has to estimate first the phases of the interacting systems and then fit a functional relationship between them. From this function, the directionality variables are then derived. The main disadvantage of this method is that it is not always possible to assign a phase to a system based on a scalar time series, especially if the power spectrum of the signal does not present a predominant peak (i.e., one cannot speak of a main frequency of rotation of the system).
2. The state-space methods are based on the relationship between neighbours in the respective phase spaces of the interacting systems X and Y. At a first glance, these methods might seem to be very close to the recurrence based method introduced in this chapter. However, there are some important differences between them. For example, the computed indices in [4, 32] are based on the mean distances between a certain number q of nearest neighbours, i.e., they use the matrix of distances $|\mathbf{x}_i - \mathbf{x}_j|$ between all points of the trajectory. In contrast, the MCR indices do not use the distance matrix explicitly but rather the matrix of inequalities $|\mathbf{x}_i - \mathbf{x}_j| < \varepsilon$. Another way to express this difference is the following: in the state-space based methods, the threshold used to compute the neighbours is different for each point of the trajectory $\mathbf{x}_i$, i.e., $\varepsilon = \varepsilon(i)$, whereas to compute MCR the threshold is the same for all points of the trajectory. Another important difference is that in the MCR method, once the threshold is fixed, it remains the same for all different values of the coupling strength. In contrast, in the

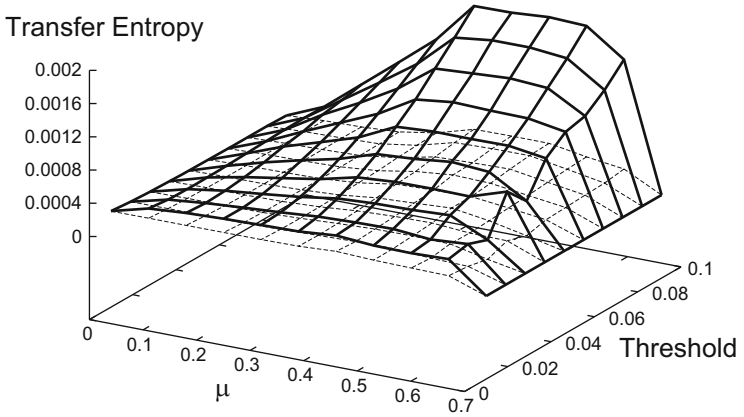

Fig. 3.9 Transfer entropy for two identical unidirectionally coupled Hénon maps in dependence on the coupling strength μ and the threshold. For each value of the coupling strength μ, the mean value over ten trajectories for uniformly distributed initial conditions has been computed. *Solid surface*: transfer entropy from X to Y, *dashed surface*: transfer entropy from Y to X

state-space based methods, the threshold does not only depend on the point of the trajectory, but also on the coupling strength.

3. Actually, the MCR method is closer to the information theory based methods, e.g., the transfer entropy [41]. In both cases, conditional probabilities of recurrence are estimated. But in the case of the transfer entropy, transition probabilities are considered, rather than static ones. This has the advantage of incorporating dynamical structure. The disadvantage compared to the MCR indices is that the number of data points needed for the estimation is considerable, and this might hamper the application of this method to experimental time series. For example, using the same number of data points (10,000) and the same range of values of the threshold as with the MCR method (Fig. 3.6) for the analysis of the direction of the coupling of [Eqs. (3.8) and (3.9)], we obtain the results for the transfer entropy as given in Fig. 3.9. The transfer entropy from X to Y is represented by the solid surface and the transfer entropy from Y to X by the dashed one. Note that even though the coupling is purely unidirectional, the transfer entropy from Y to X is larger than zero (it becomes only zero for coupling strength $\mu \geq 0.7$, when synchronisation sets in). That means that the transfer entropy does not detect that the coupling is purely unidirectional. This problem might be overcome using longer data sets. In the case of the MCR method, a purely unidirectional coupling can be easily detected by computing the recurrence rate of the driver in dependence on the coupling strength, which will then be constant.
4. A comparison between MCR and the recently introduced methods by [12,13,18] will be a subject for future work.

3.1.8 Conclusions: Part I

In this chapter, we have proposed recurrence based indices for the detection of the asymmetry of the coupling between interacting systems. The quantification of the asymmetry of the coupling can be very helpful in identifying driver-response relationships, which is a relevant problem in many fields, especially when dealing with experimental time series. The proposed indices are based on the mean conditional probabilities of recurrence (MCR). We have exemplified their applicability by several numerical examples which are representative of strong and weak coupled systems. Furthermore, we have shown that the MCR indices can also cope with the more challenging case of structurally different systems. We have studied the dependence of the MCR indices on the parameters needed for their estimation and we have found out that the choice of the parameters is not crucial for the correct detection of the asymmetry of the coupling. Moreover, we have addressed the very relevant problem of the quantification of the direction of the coupling in passive experiments and proposed an algorithm to assess the statistical significance of the results. Furthermore, we have studied the influence of observational noise on our method and compared it with other existing techniques for the detection of the asymmetry of the coupling. The numerical examples we considered in this chapter were mainly low dimensional. This technique is promising as shown by an application to experimental time series in the cardio-respiratory system [23].

3.2 Part II: Inferring Indirect Coupling

3.2.1 Introduction: Part II

The first part of this chapter introduced a new method to detect and quantify the asymmetry of the coupling between two interacting systems based on their recurrence properties [33]. Originally, it has focused on bivariate situations. It is crucial to extend it to multivariate time series analysis as this occurs quite often in many real applications. Inferring the coupling configuration at a local scale can be of substantial help to explain the global functioning of the network, e.g., the finding of motifs can be crucial for the understanding of the whole system [3, 44]. Therefore, now we focus on the inference of the coupling configuration of small networks consisting of three nodes.

Let us start considering the following small network as in Fig. 3.10, showing six different coupling settings for three unidirectionally interacting nodes. A pairwise analysis (bivariate) is often insufficient in addressing the possible indirect coupling (e.g., the coupling between X and Z in Fig. 3.10d). Hence, one main objective here is to identify the indirect coupling by means of recurrences. More specifically, we will identify the difference among these six coupling cases by studying the recurrence properties. The advantage of the extension from two to three coupled

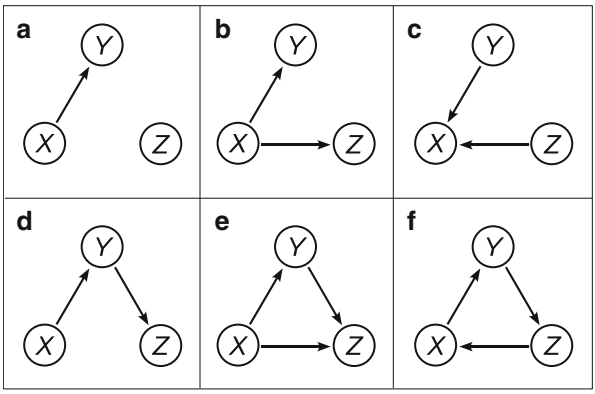

Fig. 3.10 Coupling configuration settings for three systems, that only uni-directional couplings are considered. (**a**) Z is independent of both X and Y. (**b**) X is the common driver for both Y and Z. (**c**) X is co-regulated by Y and Z. (**d**) X drives Y, while Y further drives Z. (**e**) Direct coupling with X being the common driver and Z being the common response. (**f**) Direct coupling in a ring way

systems is that it makes possible to analyze data measured from small networks, such as the EEG recordings on the scalp, so frequently used in neuroscience and cognitive psychology. In such experimental situations we have access to time series from typically of the order of ten nodes. Furthermore, it is crucial to identify the indirect coupling between X and Z as illustrated by Fig. 3.10d since it is one of big challenges for multivariate analysis. Therefore, we extend the study of [33] to three oscillators.

We show numerical studies for the application to three coupled Lorenz systems with six different coupling configurations (Fig. 3.10). Specifically, we consider the following system

$$X: \begin{cases} \dot{x}_1 = \sigma(x_2 - x_1), \\ \dot{x}_2 = r x_1 - x_2 - x_1 x_3 + \mu_{21} y_2^2 + \mu_{31} z_3^2, \\ \dot{x}_3 = x_1 x_2 - b x_3, \end{cases} \tag{3.15}$$

$$Y: \begin{cases} \dot{y}_1 = \sigma(y_2 - y_1), \\ \dot{y}_2 = r y_1 - y_2 - y_1 y_3 + \mu_{12} x_2^2 + \mu_{32} z_3^2, \\ \dot{y}_3 = y_1 y_2 - b y_3, \end{cases} \tag{3.16}$$

$$Z: \begin{cases} \dot{z}_1 = \sigma(z_2 - z_1), \\ \dot{z}_2 = r z_1 - z_2 - z_1 z_3 + \mu_{13} x_2^2 + \mu_{23} y_2^2, \\ \dot{z}_3 = z_1 z_2 - b z_3. \end{cases} \tag{3.17}$$

Table 3.1 Variation of *RR* of each individual system

	(a)	(b)	(c)	(d)	(e)	(f)
RR_X	−	−	+	−	−	+
RR_Y	+	+	−	+	+	+
RR_Z	−	+	−	+	+	+

The symbols "+" correspond to the existence of variation, while "−" means there is no changes with increasing coupling strength

We integrate these equations numerically by a step 0.003 with sampling every 100 points leading to time step $\Delta t = 0.3$. We use standard parameters $\sigma = 10, r = 28, b = 8/3$ as in the uncoupled case $\mu_{i,j} = 0$ so that the oscillators are in a chaotic regime.

Our procedure to deal with the six coupling settings of Fig. 3.10 has three steps, which are explained in different sections: in Sect. 3.2.2, we apply a univariate analysis, namely analyzing each individual system separately; in Sect. 3.2.3, we perform a pairwise analysis, after which only the coupling configuration of Fig. 3.10d, e remains unclear. In Sect. 3.2.4, the partial mean conditional probability of recurrence is developed to cope with the last two remaining cases. Some conclusions are drawn in Sect. 3.2.7.

3.2.2 First Step: Univariate Analysis

Given the recurrence matrix Eq. (3.1), we are particularly interested in the mean probability of recurrence (recurrence rate), which is estimated by

$$\left\langle p(x_j)\right\rangle = RR = \frac{1}{N^2}\sum_{i,j=1}^{N} R_{i,j}\,. \tag{3.18}$$

The first step is to study the variations of the mean probability of recurrences with respect to an increase of the coupling strength (Fig. 3.10), separately. For instance, in the case of coupling as in Fig. 3.10a, both $\langle p(x)\rangle$ and $\langle p(z)\rangle$ remain unchanged while $\langle p(y)\rangle$ varies if the coupling strength μ is increased. This is because Z is independent of X and Y and the coupling from X to Y is unidirectional. A similar analysis can be achieved for each coupling setting of Fig. 3.10. We summarize the result in Table 3.1. We note that, throughout the chapter, the symbol "+" correspond to a change of the recurrence rate of the component, while "−" means there is no change with increasing the coupling strength. Furthermore "(a), . . ., (f)" denote the six different coupling configurations, as shown in Fig. 3.10.

The numerical simulation for the first step is shown in Fig. 3.11, which verifies the results presented in Table 3.1. By the first step of the univariate analysis, six different couplings are subdivided into three categories: $(+,-,-)$, $(+,+,-)$, and

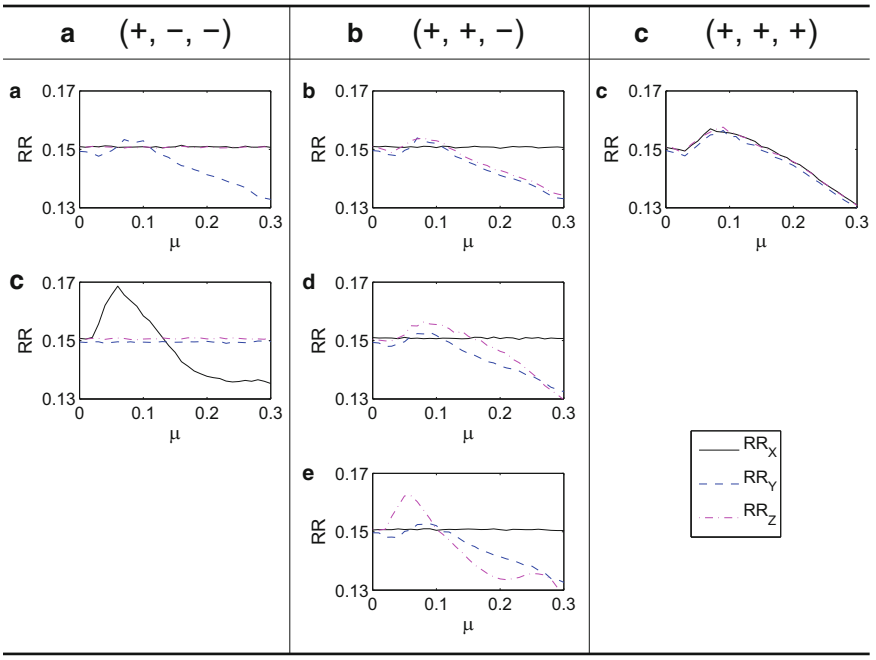

Fig. 3.11 Univariate analysis. Six coupling cases are classified into three groups A, B and C according to our univariate analysis

$(+,+,+)$. Note that $(+,-,-)$ denotes the configurations for which only the *RR* of one component changes with the coupling strength no matter which component. Therefore, the coupling configurations (a) and (c) are classified in the same group A.

Note that in principle one could also use other measures from Recurrence Quantification Analysis (RQA) [21] for this first step analysis (cf. Chap. 1). However it is not clear whether their use would allow identifying the coupling configuration. Moreover, the interpretation of the results might be difficult and rather empirical. Nevertheless, it is important to note that the probability of recurrence has a deep theoretical meaning as it is the basis for calculating many dynamical invariants, i.e., correlation dimension D_2 [17]. Furthermore, it has a clear relationship with information theoretic approaches (see [28]).

3.2.3 Second Step: Pairwise Analysis

In the second step, we perform a pairwise analysis, which is a generalisation of the RPs to joint recurrence plots (JRPs), namely calculating Eq. (3.2).

Based on the results obtained in the first step (Table 3.1 and Fig. 3.15), we do the pairwise analysis for cases A and B, following the notation of Fig. 3.11 since in

case C we have only one coupling configuration. Furthermore, we characterize the results of the pairwise analysis using the same notations as before. For instance, if $\Delta MCR(X|Y)$ changes with the coupling strength whereas $\Delta MCR(X|Z)$ and $\Delta MCR(Y|Z)$ stay constant, we write $(+,-,-)$. In particular, we have explicit expressions for Eq. (3.1.2) for each coupling:

A: couplings (a) and (c)

(a): $(+,-,-)$

$$\Delta MCR(Y|X) > 0, \tag{3.19}$$

$$\Delta MCR(Z|X) = RR_Z - RR_X \approx 0, \tag{3.20}$$

$$\Delta MCR(Z|Y) = RR_Y - RR_Z. \tag{3.21}$$

Note that RR_Y changes with the coupling strength, leading to $\Delta MCR(Z|Y) < 0$. However, $\Delta MCR(Z|Y)$ simply follows the same curve of univariate analysis since Y is independent of Z. In this respect, we denote it as "−".

(c): $(+,+,-)$

$$\Delta MCR(Y|X) < 0, \tag{3.22}$$

$$\Delta MCR(Z|X) < 0, \tag{3.23}$$

$$\Delta MCR(Z|Y) = RR_Z - RR_Y \approx 0. \tag{3.24}$$

B: couplings (b), (d) and (e)

(b): $(+,+,-)$

$$\Delta MCR(Y|X) > 0, \tag{3.25}$$

$$\Delta MCR(Z|X) > 0, \tag{3.26}$$

$$\Delta MCR(Z|Y) \approx 0. \tag{3.27}$$

(d, e): $(+,+,+)$

$$\Delta MCR(Y|X) > 0, \tag{3.28}$$

$$\Delta MCR(Z|X) > 0, \tag{3.29}$$

$$\Delta MCR(Z|Y) > 0. \tag{3.30}$$

Therefore, after the pairwise analysis, only the cases (d) and (e) remain ambiguous.

The numerical simulations for the pairwise analysis of the second step are shown in Fig. 3.12 for (a, c), and Fig. 3.13 for (b, d, e), respectively.

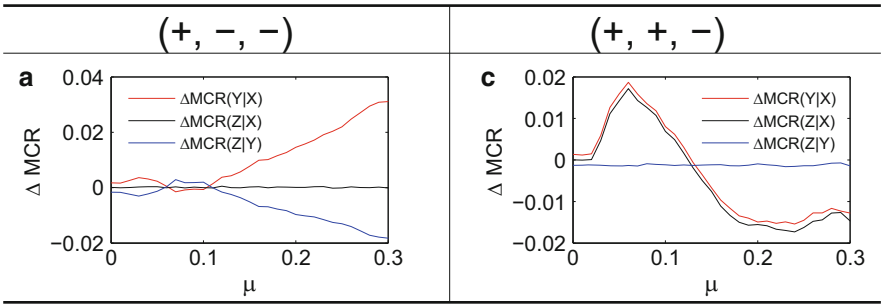

Fig. 3.12 Pairwise comparison for coupling (*a*, *c*). The *left panel* is for coupling configuration (*a*), the *right panel* is for coupling configuration (*c*). Note that in (*a*), $\Delta MCR(Z|Y)$ is completely overlapped with the difference between RR_Y and RR_Z, which can be obtained from the first step of univariate analysis (see Fig. 3.11)

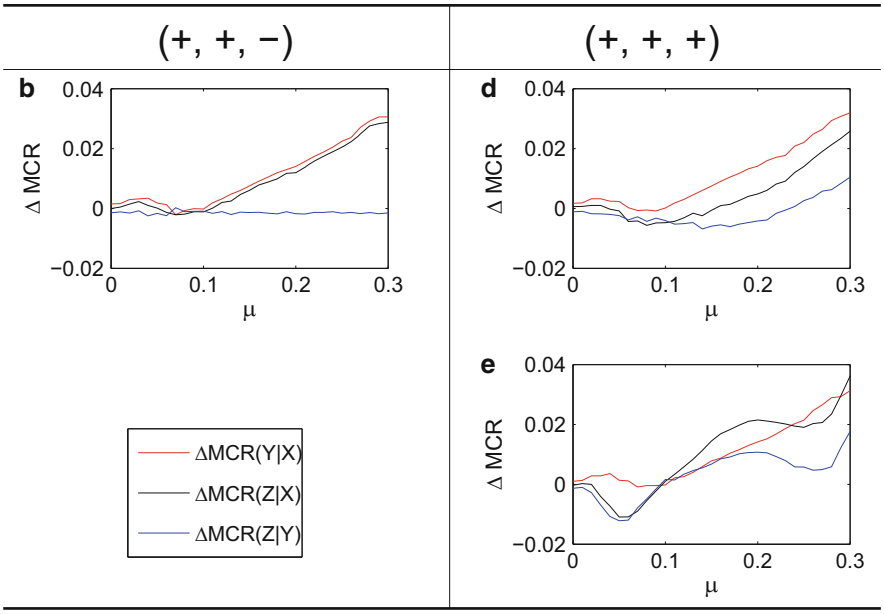

Fig. 3.13 Pairwise comparison for coupling configurations (*b*, *d*, *e*). The *left panel* is for (*b*), the *right panel* is for coupling configurations (*d*, *e*)

3.2.4 Third Step: Partial MCR

A recurrence-based bivariate analysis is generally not conclusive in addressing the existence of indirect coupling. Hence, we go to the crucial step in extending the method to deal with the remaining two coupling cases (d) and (e) after the previous two steps.

Let us first consider *MCR* of two variables used in our previous bivariate analysis, i.e., the pair of X and Y. We calculate $MCR(Y|X)$ and $MCR(X|Y)$, respectively. The second step is to quantify the influence of the third variable Z on $MCR(Y|X)$ by considering the difference between $MCR(Y|X)$ and the mean conditional probability of recurrence that Y recurs given that *both* X and Z recur,

$$\Delta MCR(Y|X)_Z = -\big(MCR(Y|X) - MCR(Y|X,Z)\big). \tag{3.31}$$

Similarly the contribution of Z to the $MCR(X|Y)$ is calculated by

$$\Delta MCR(X|Y)_Z = -\big(MCR(X|Y) - MCR(X|Y,Z)\big). \tag{3.32}$$

Before synchronisation sets in, we have $MCR(Y|X) < MCR(Y|X,Z)$ due to $\langle p(\mathbf{x}_j)\rangle > \langle p(\mathbf{x}_j,\mathbf{z}_j)\rangle$. Hence, for convenience the normalization factor (negative symbol) in front of the right hand side in Eq. (3.31) is introduced to keep the probability values to be positive. Note that $\Delta MCR(Y|X)_Z$ quantifies a subset of $MCR(Y|X)$, measuring the contribution of Z to the probabilities of recurrence of Y via X. In this regard, we call $\Delta MCR(Y|X)_Z$ *partial MCR*. Moreover, in general $\Delta MCR(Y|X)_Z$ is different from $\Delta MCR(X|Y)_Z$ because of the asymmetry between $MCR(Y|X)$ and $MCR(X|Y)$.

Analogously, the contribution of Y to $MCR(Z|X)$ and $MCR(X|Z)$ is calculated, respectively, by

$$\Delta MCR(Z|X)_Y = -\big(MCR(Z|X) - MCR(Z|X,Y)\big), \tag{3.33}$$

$$\Delta MCR(X|Z)_Y = -\big(MCR(X|Z) - MCR(X|Y,Z)\big). \tag{3.34}$$

The contribution of X to $MCR(Y|Z)$ and $MCR(Z|Y)$ is computed by

$$\Delta MCR(Y|Z)_X = -\big(MCR(Y|Z) - MCR(Y|X,Z)\big), \tag{3.35}$$

$$\Delta MCR(Z|Y)_X = -\big(MCR(Z|Y) - MCR(Z|X,Y)\big). \tag{3.36}$$

Depending on the particular coupling configuration (Fig. 3.10a–f), we obtain explicit expressions for measuring the contribution of one system to the other two. The details are presented in Sect. 3.2.6. In this section, however, we focus on the remaining two coupling configurations that have still to be distinguished, namely (d) and (e).

(d) From the viewpoint of Z, the contribution of indirect coupling from X to Z is smaller than that of the direct coupling from Y to Z. Hence $MCR(Z|X) < MCR(Z|Y)$ and considering Eqs. (3.33) and (3.36) we have

$$\Delta MCR(Z|Y)_X < \Delta MCR(Z|X)_Y. \tag{3.37}$$

This is validated by showing a similar relationship from the X perspective, namely, $MCR(X|Z) < MCR(X|Y)$ implying

$$\Delta MCR(X|Y)_Z < \Delta MCR(X|Z)_Y. \tag{3.38}$$

However, from the mediator Y viewpoint, one has

$$\Delta MCR(Y|X)_Z \lessapprox \Delta MCR(Y|Z)_X, \tag{3.39}$$

indicating Y to be a mediator.

(e) In this case, from the perspective of system Z, the contribution of X to Z is larger than the contribution of Y to Z, which implies $MCR(Z|Y) < MCR(Z|X)$. This yields, considering again Eqs. (3.33) and (3.36),

$$\Delta MCR(Z|X)_Y < \Delta MCR(Z|Y)_X. \tag{3.40}$$

This relationship is validated from the X perspective, $MCR(X|Y) < MCR(X|Z)$, implying

$$\Delta MCR(X|Z)_Y < \Delta MCR(X|Y)_Z. \tag{3.41}$$

Moreover, from the viewpoint of Y, we have

$$\Delta MCR(Y|Z)_X < \Delta MCR(Y|X)_Z. \tag{3.42}$$

The numerical simulations for the partial *MCR* analysis for the coupling configurations (d, e) involved in the third step are shown in Fig. 3.14, which agree with our theoretical expectation in a reasonable range for coupling strengths.

3.2.5 Decision Tree

Following the discussions presented in previous sections, we conclude that the six different coupling configurations are clearly identified with our three-step procedure (plotted as a decision tree in Fig. 3.15):

1. Univariate analysis, namely the probability of recurrences for each individual systems, identifies the coupling configuration of (f). Note that couplings (a, c) are not able to be further classified because of the relabeling.
2. Pairwise analysis, allows distinguishing the coupling configuration of (a) from (c), and (b) from (d, e).
3. Partial *MCR* analysis identifies the difference between coupling (d) and (e).

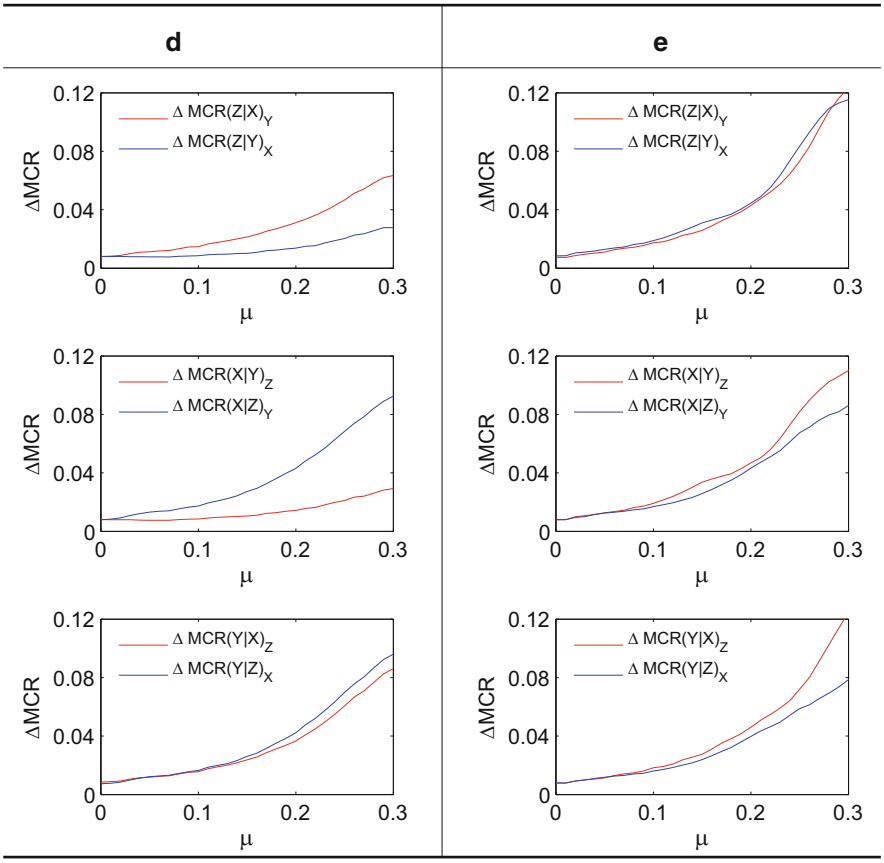

Fig. 3.14 Partial *MCR* shows distinct behavior for the coupling configurations (*d*) and (*e*)

3.2.6 *Partial MCR for All Couplings of Fig. 3.10*

The detailed analysis for the partial *MCR* for the coupling settings in Fig. 3.10 is performed in this section. We assume that the three systems are identical in the case of zero coupling and that the coupling strengths can be changed systematically, which is often the case for many active experiments. Note that the numerical results are based on Eqs. (3.15)–(3.17)).

(a) Z independent of both X *and* Y (Fig. 3.10a)
We obtain $MCR(Y|(X,Z)) = MCR(Y|X)$. This means that the contribution of Z to $MCR(Y|X)$ can be disregarded. Similarly, we have $MCR(X|(Y,Z)) = MCR(X|Y)$. Furthermore, $MCR(Z|X) = RR_Z$, $MCR(Z|X,Y) = RR_Z$, and $MCR(Y|Z) = RR_Y$ since Z is independent of both X and Y. Explicitly we have the following equations:

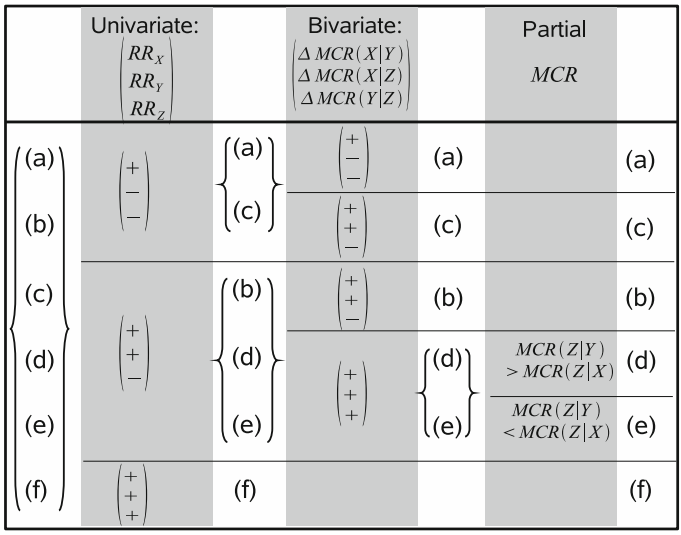

Fig. 3.15 Decision tree derived from the theoretical analysis. Our procedure consists of three steps, namely univariate, pairwise and partial *MCR* analysis

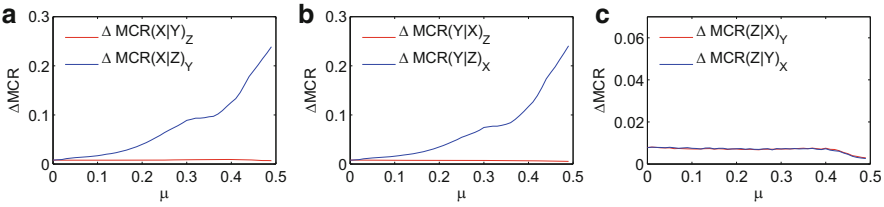

Fig. 3.16 Z independent of both X and Y (Fig. 3.10a, $\mu_{12} = \mu, \mu_{ij} = 0$ otherwise). (**a**) From the viewpoint of X, $\Delta MCR(X|Y) = 0$, Eq. (3.43). (**b**) $\Delta MCR(Y|X)_Z = 0$, Eq. (3.45). However, due to the finite length of the time series used, these curves show some deviations from zero ($\mu = 0$). (**c**) $\Delta MCR(Z|Y)_X \approx 0, \Delta MCR(Z|X) \approx 0$

$$\Delta MCR(X|Y)_Z = 0, \tag{3.43}$$

$$\Delta MCR(X|Z)_Y = -\big(RR_X - MCR(X|Y)\big), \tag{3.44}$$

$$\Delta MCR(Y|X)_Z = 0, \tag{3.45}$$

$$\Delta MCR(Y|Z)_X = -\big(RR_Y - MCR(Y|X)\big), \tag{3.46}$$

$$\Delta MCR(Z|X)_Y = 0, \tag{3.47}$$

$$\Delta MCR(Z|Y)_X = 0. \tag{3.48}$$

In general [Eqs. (3.44) and (3.46)] are not equal because of the asymmetry between X and Y. Figure 3.16 shows the numerical result.

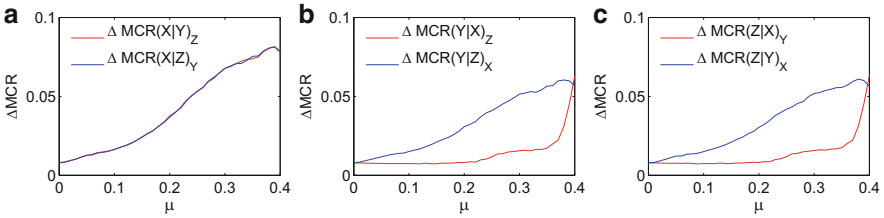

Fig. 3.17 (**a**) X is the common driver for both Y and Z (Fig. 3.10b, $\mu_{12} = \mu_{13} = \mu$, $\mu_{ij} = 0$ otherwise). (**b**) From X viewpoint, $\Delta MCR(Y|X)_Z < \Delta MCR(Y|Z)_X$, Eq. (3.52). (**c**) The same holds for Eq. (3.53), verified by $\Delta MCR(Z|X)_Y < \Delta MCR(Z|Y)_X$. Note that when $\mu > 0.39$, Y is synchronized with X suggested by the Lyapunov exponent spectrum (not shown here).

(b) X is a common driver (Fig. 3.10b)
From the viewpoint of X, $MCR(X|Y) = MCR(X|Z)$, since Y and Z are identical. Hence we have

$$\Delta MCR(X|Y)_Z = \Delta MCR(X|Z)_Y. \tag{3.49}$$

It is also obvious to see that Y is independent of Z under the condition of X, yielding $MCR(Y|Z) = RR_Y$, $MCR(Z|Y) = RR_Z$, thus,

$$\Delta MCR(Y|Z)_X = -\big(RR_Y - MCR(Y|X,Z)\big), \tag{3.50}$$

$$\Delta MCR(Z|Y)_X = -\big(RR_Z - MCR(Z|X,Y)\big). \tag{3.51}$$

In general before reaching synchronisation we have the mean recurrence probability relationship $\langle p(\mathbf{x}_j)\rangle > \langle p(\mathbf{y}_j)\rangle \approx \langle p(\mathbf{z}_j)\rangle$, $\langle p(\mathbf{x}_j, \mathbf{y}_j)\rangle > \langle p(\mathbf{y}_j, \mathbf{z}_j)\rangle = \langle p(\mathbf{y}_j)\rangle \cdot \langle p(\mathbf{z}_j)\rangle$. Hence, $MCR(Y|X) > MCR(Y|Z) = RR_Y$, which leads to

$$\Delta MCR(Y|X)_Z < \Delta MCR(Y|Z)_X. \tag{3.52}$$

The same holds from the viewpoint of Z, namely,

$$\Delta MCR(Z|X)_Y < \Delta MCR(Z|Y)_X. \tag{3.53}$$

Figure 3.17 shows the numerical results.

(c) X is a common response (Fig. 3.10c)
When X is the common receiver, Y and Z are independent of each other. Hence, we derive the same theoretical results as the case that X is the common driver. Particularly, we have

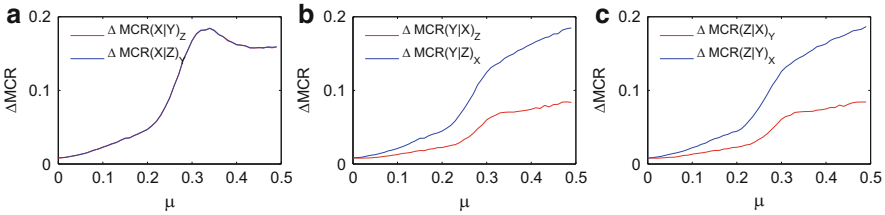

Fig. 3.18 X is the common receiver for both Y and Z (Fig. 3.10c, $\mu_{21} = \mu_{31} = \mu$, $\mu_{ij} = 0$ otherwise). Equations (3.54)–(3.56) are verified (see the caption of Fig. 3.17)

$$\Delta MCR(X|Y)_Z = \Delta MCR(X|Z)_Y, \tag{3.54}$$

$$\Delta MCR(Y|X)_Z < \Delta MCR(Y|Z)_X, \tag{3.55}$$

$$\Delta MCR(Z|X)_Y < \Delta MCR(Z|Y)_X. \tag{3.56}$$

Figure 3.18 shows the numerical results.

(d) Z indirectly coupled with X, but directly driven by Y (Fig. 3.10d)
Because of the asymmetry of $MCR(Y|X)$ and $MCR(X|Y)$, one expects the difference between $\Delta MCR(Y|X)_Z$ and $\Delta MCR(X|Y)_Z$. More specifically, the values of [Eqs. (3.31)–(3.36)] are not zero.

Note that within the coupling setting (Fig. 3.10d), we have $\langle p(\mathbf{x}_j)\rangle > \langle p(\mathbf{y}_j)\rangle > \langle p(\mathbf{z}_j)\rangle$. Before synchronisation (neither two subsystems are synchronized), $\langle p(\mathbf{x}_j)\rangle > \langle p(\mathbf{y}_j, \mathbf{z}_j)\rangle$, $\langle p(\mathbf{y}_j)\rangle > \langle p(\mathbf{x}_j, \mathbf{z}_j)\rangle$, and $\langle p(\mathbf{z}_j)\rangle > \langle p(\mathbf{x}_j, \mathbf{y}_j)\rangle$. Furthermore, the complexity of (X, Z) is greater than the complexity of the joint space of (Y, Z). This leads to the joint recurrence probability of $\langle p(\mathbf{y}_j, \mathbf{z}_j)\rangle$ being greater than $\langle p(\mathbf{x}_j, \mathbf{z}_j)\rangle$. Hence we have $MCR(Z|Y) > MCR(Z|X)$, which yields

$$\Delta MCR(Z|Y)_X < \Delta MCR(Z|X)_Y. \tag{3.57}$$

From the viewpoint of Z, the relationship of the inequality of equation (3.57) suggests that the contribution of indirect coupling from X to Z is smaller than that of the direct coupling from Y to Z. This is validated by showing a similar relationship from the X perspective, namely,

$$\Delta MCR(X|Y)_Z < \Delta MCR(X|Z)_Y. \tag{3.58}$$

However from the mediator Y viewpoint, it sends out the coupling information to Z when receiving the same amount of information from X. Hence, one has

$$\Delta MCR(Y|X)_Z \lessapprox \Delta MCR(Y|Z)_X, \tag{3.59}$$

indicating Y to be the mediator. Figure 3.19 shows the numerical results.

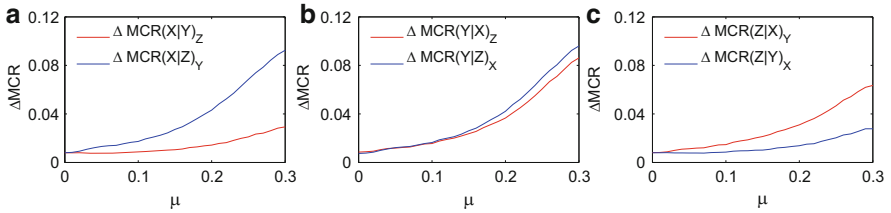

Fig. 3.19 X drives Y, and Y drives Z (Fig. 3.10d, $\mu_{12} = \mu_{23} = \mu$, $\mu_{ij} = 0$ otherwise). (**a**) $\Delta MCR(X|Y)_Z < \Delta MCR(X|Z)_Y$, (**c**) $\Delta MCR(Z|Y)_X < \Delta MCR(Z|X)_Y$. (**b**) However, Y is a mediator, having $\Delta MCR(Y|X)_Z \lessapprox \Delta MCR(Y|Z)_X$

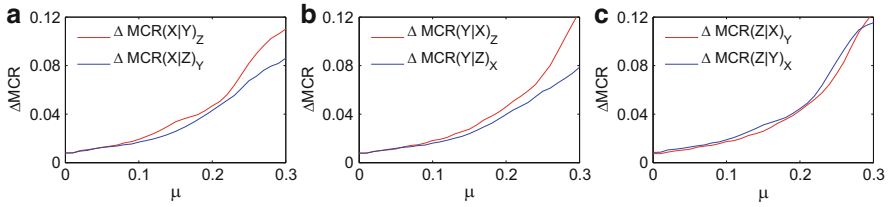

Fig. 3.20 X drives both Y and Z, and Y drives Z (Fig. 3.10e, $\mu_{12} = \mu_{13} = \mu_{23} = \mu$, $\mu_{ij} = 0$ otherwise). (**a**) $\Delta MCR(X|Z)_Y < \Delta MCR(X|Y)_Z$. (**b**) $\Delta MCR(Y|Z)_X < \Delta MCR(Y|X)_Z$ holds before synchronisation. (**c**) $\Delta(Z|X)_Y < \Delta(Z|Y)_X$

(e) Direct coupling setting: X is the common driver and Z is the common receiver (Fig. 3.10e)
From the perspective of system X, both Y and Z have the same contribution to X, namely, we have

$$\Delta MCR(X|Z)_Y < \Delta MCR(X|Y)_Z. \tag{3.60}$$

From the viewpoint of Z, it accepts two packages of information from the driver X. One is from the direct contribution sent by X to Z; the other is received via the mediator Y. Z cannot distinguish where these two packages of information come from. Therefore, we have

$$\Delta MCR(Z|X)_Y < \Delta MCR(Z|Y)_X, \tag{3.61}$$

indicating that the transitivity property of Y is identified. Before onset of synchronisation, we again have $\langle p(\mathbf{x}_j)\rangle > \langle p(\mathbf{y}_j)\rangle > \langle p(\mathbf{z}_j)\rangle$. Further, the relationship of $\langle p(\mathbf{x}_j, \mathbf{y}_j)\rangle > \langle p(\mathbf{y}_j, \mathbf{z}_j)\rangle$ holds. Hence, from the viewpoint of Y, we have

$$\Delta MCR(Y|Z)_X < \Delta MCR(Y|X)_Z. \tag{3.62}$$

Figure 3.20 shows the numerical results.

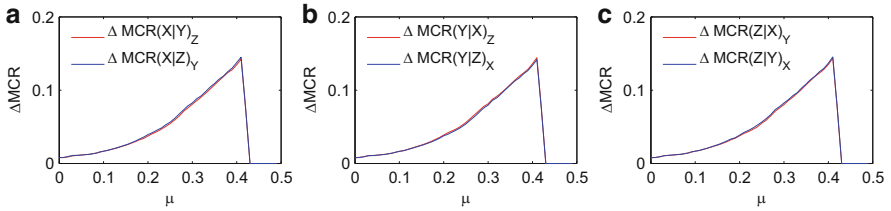

Fig. 3.21 X drives Y, Y drives Z, and Z drives X (Fig. 3.10f, $\mu_{12} = \mu_{23} = \mu_{31} = \mu$, $\mu_{ij} = 0$ otherwise) [Eqs. (3.63)–(3.65)]

(f) Direct coupling setting: in a ring way (Fig. 3.10f)
All measures are the same, since each system shows basically the same recurrence behavior, namely,

$$\Delta MCR(X|Y)_Z = \Delta MCR(X|Z)_Y, \tag{3.63}$$

$$\Delta MCR(Y|X)_Z = \Delta MCR(Y|Z)_X, \tag{3.64}$$

$$\Delta MCR(Z|X)_Y = \Delta MCR(Z|Y)_X. \tag{3.65}$$

Note that this only holds in the case when the three systems are identical, yielding the same transitivity ability. Figure 3.21 shows the numerical results.

3.2.7 *Conclusions: Part II*

We have shown a generalisation of *MCR* to three coupled systems, in particular including the extraction of indirect coupling. We have demonstrated our procedure using three Lorenz oscillators in chaotic regime in six different coupling configurations. Some issues might appear in the line of experimental studies, which have to be taken into consideration. Noise is ubiquitous in experimental time series and requires developing robust measures to identify the correct coupling configuration. It has been demonstrated that most recurrence structures are preserved if the free parameter ϵ (threshold in the recurrence matrix Eq. (3.1)) is chosen as $\epsilon \approx 5\sigma$, where σ corresponds to the standard deviation of the observational noise [48]. For the application to a large network of coupled units, the method has to be adapted to keep a good statistical power and to reduce the computation time. A further issue that will be considered in the future is the presence of asymmetric bidirectional coupling, as it is rather common in experimental complex networks.

Acknowledgements This work has been partially funded by the Federal Ministry for Education and Research (BMBF) via the Potsdam Research Cluster for Georisk Analysis, Environmental Change and Sustainability (PROGRESS), the National Natural Science Foundation of China (Grant No. 11305062, 11135001, 11075056), Specialized Research Fund for the Doctoral Program

(20130076120003), the Innovation Program of Shanghai Municipal Education Commission under grant No. 12ZZ043, SRF for ROCS, SEM, and the Hong Kong Polytechnic University Postdoctoral Fellowship. We acknowledge the discussion with N. Marwan, and M. Small.

References

1. V. Afraimovich, Pesin's dimension for Poincaré recurrences. Chaos **7**(1), 12–20 (1997)
2. R. Albert, A.L. Barabasi, Statistical mechanics of complex networks. Rev. Mod. Phys. **74**(1) (2002). doi:10.1103/RevModPhys.74.47
3. U. Alon, *An Introduction to Systems Biology: Design Principles of Biological Circuits*. Chapman & Hall/CRC Mathematical & Computational Biology (Chapman & Hall, Boca Raton, 2006)
4. J. Arnhold, K. Lehnertz, P. Grassberger, C.E. Elger, A robust method for detecting interdependences: application to intracranially recorded EEG. Physica D **134**, 419 (1999)
5. A. Bahraminasab, F. Ghasemi, A. Stefanovska, P.V.E. McClintock, H. Kantz, Direction of coupling from phases of interacting oscillators: a permutation information approach. Phys. Rev. Lett. **100**(8), 084101 (2008)
6. S. Boccaletti, J. Kurths, G. Osipovd, D.L. Valladaresb, C.S. Zhou, The synchronization of chaotic systems. Phys. Rep. **366**(1–2), 1–101 (2002)
7. M. Ding, Y. Chen, S.L., in *Bressler, Granger Causality, Basic Theory and Application to Neuroscience*, ed. by B. Schelter, M. Winterhalder, J. Timmer. Handbook of Time Series Analysis (Wiley-VCH Verlag GmbH & Co. KGaA, Weinheim, 2007), pp. 437–460
8. J. Donges, Y. Zou, N. Marwan, J. Kurths, The backbone of the climate network. Europhys. Lett. **87**(4), 48,007 (2009)
9. J.F. Donges, Y. Zou, N. Marwan, J. Kurths, Complex networks in climate dynamics: comparing linear and nonlinear network construction methods. Eur. Phys. J. ST **174**, 157–179 (2009)
10. J.P. Eckmann, S.O. Kamphorst, D. Ruelle, Recurrence plots of dynamical systems. Europhys. Lett. **4**(9), 973–977 (1987)
11. P. Faure, H. Korn, A new method to estimate the kolmogorov entropy from recurrence plots: its application to neuronal signals. Physica D **122**(1–4), 265–279 (1998). doi:10.1016/S0167-2789(98)00177-8
12. J.H. Feldhoff, R.V. Donner, J.F. Donges, N. Marwan, J. Kurths, Geometric detection of coupling directions by means of inter-system recurrence networks. Phys. Lett. A **376**(46), 3504–3513 (2012). doi:http://dx.doi.org/10.1016/j.physleta.2012.10.008
13. J.H. Feldhoff, R.V. Donner, J.F. Donges, N. Marwan, J. Kurths, Geometric signature of complex synchronisation scenarios. Europhys. Lett. (EPL) **102**(3), 30,007 (2013)
14. S. Frenzel, B. Pompe, Partial mutual information for coupling analysis of multivariate time series. Phys. Rev. Lett. **99**(20), 204101 (2007)
15. R. Gilmore, M. Lefranc, in *The Topology of Chaos: Alice in Stretch and Squeezeland* (Wiley, New York, 2002)
16. C.W.J. Granger, Investigating causal relations by econometric models and cross-spectral methods. Econometrica **37**(3), 424–438 (1969)
17. P. Grassberger, I. Procaccia, Characterization of strange attractor Phys. Rev. Lett. **50**(5), 346–349 (1983)
18. Y. Hirata, K. Aihara, Identifying hidden common causes from bivariate time series: a method using recurrence plots. Phys. Rev. E **81**, 016,203 (2010). doi:10.1103/PhysRevE.81.016203
19. H. Kantz, T. Schreiber, in *Nonlinear Time Series Analysis*, 2nd edn. (Cambridge University Press, Cambridge, 2004)
20. L. Kocarev, U. Parlitz, Generalized synchronization, predictability, and equivalence of unidirectionally coupled dynamical systems. Phys. Rev. Lett. **76**(11), 1816–1819 (1996)

21. N. Marwan, M. Romano, M. Thiel, J. Kurths, Recurrence plots for the analysis of complex systems. Phys. Rep. **438**(5–6), 237–329 (2007)
22. N. Marwan, N. Wessel, U. Meyerfeldt, A. Schirdewan, J. Kurths, Recurrence plot based measures of complexity and its application to heart rate variability data. Phys. Rev. E **66**(2), 026,702 (2002)
23. N. Marwan, Y. Zou, N. Wessel, M. Riedl, J. Kurths, Estimating coupling directions in the cardiorespiratory system using recurrence properties. Philos. Trans. R. Soc. A Math. Phys. Eng. Sci. **371**(1997) (2013). doi:10.1098/rsta.2011.0624
24. J. Nawrath, M.C. Romano, M. Thiel, I.Z. Kiss, M. Wickramasinghe, J. Timmer, J. Kurths, B. Schelter, Distinguishing direct from indirect interactions in oscillatory networks with multiple time scales. Phys. Rev. Lett. **104**(3), 038,701 (2010). doi:10.1103/PhysRevLett.104.038701
25. H. Osterhage, F. Mormann, T. Wagner, K. Lehnertz, Detecting directional coupling in the human epileptic brain: limitations and potential pitfalls. Phys. Rev. E **77**(1), 011914 (2008)
26. M. Palus, V. Komarek, Z. Hrncir, K. Sterbova, Synchronization as adjustment of information rates: detection from bivariate time series. Phys. Rev. E **63**, 046,211 (2001)
27. M. Palus, A. Stefanovska, Direction of coupling from phases of interacting oscillators: an information-theoretic approach. Phys. Rev. E **67**, 055,201(R) (2003)
28. M. Paluš, M. Vejmelka, Directionality of coupling from bivariate time series: how to avoid false causalities and missed connections. Phys. Rev. E **75**(5), 056211 (2007)
29. A. Pikovsky, M. Rosenblum, J. Kurths, in *Synchronization: A Universal Concept in Nonlinear Sciences*. (Cambridge University Press, Cambridge, 2001)
30. H. Poincaré, Sur la probleme des trois corps et les équations de la dynamique. Acta Math. **13**, 1–271 (1890)
31. A. Porta, G. Baselli, N. Montano, T. Gnecchi-Ruscone, F. Lombardi, A. Malliani, S. Cerutti, Classification of coupling patterns among spontaneous rhythms and ventilation in the sympathetic discharge of decerebrate cats. Biol. Cybern. **75**(2), 163–172 (1996). doi:10.1007/s004220050284
32. R.Q. Quiroga, J. Arnhold, P. Grassberger, Learning driver-response relationships from synchronization patterns. Phys. Rev. E **61**(5), 5142–5148 (2000)
33. M.C. Romano, M. Thiel, J. Kurths, C. Grebogi, Estimation of the direction of the coupling by conditional probabilities of recurrence. Phys. Rev. E **76**(3), 036211 (2007)
34. M.C. Romano, M. Thiel, J. Kurths, I.Z. Kiss, J. Hudson, Detection of synchronization for non-phase-coherent and non-stationary data. Europhys. Lett. **71**(3), 466–472 (2005)
35. M.C. Romano, M. Thiel, J. Kurths, K. Mergenthaler, R. Engbert, Hypothesis test for synchronization: twin surrogates revisited. Chaos **19**(1), 015,108 (2009). http://link.aip.org/link/?CHA/19/015108/1
36. M.C. Romano, M. Thiel, J. Kurths, W. von Bloh, Multivariate recurrence plots. Phys. Lett. A **330**(3–4), 214–223 (2004)
37. M.G. Rosenblum, L. Cimponeriu, A. Bezerianos, A. Patzak, R. Mrowka, Identification of coupling direction: application to cardiorespiratory interaction. Phys. Rev. E **65**(4), 041909 (2002)
38. M.G. Rosenblum, A.S. Pikovsky, Detecting direction of coupling in interacting oscillators. Phys. Rev. E **64**(4), 045202 (2001)
39. N.F. Rulkov, M.M. Sushchik, L.S. Tsimring, H.D.I. Abarbanel, Generalized synchronization of chaos in directionally coupled chaotic systems. Phys. Rev. E **51**(2), 98–994 (1995)
40. B. Saussol, J. Wu, Recurrence spectrum in smooth dynamical systems. Nonlinearity **16**(6), 1991–2001 (2003)
41. T. Schreiber: Measuring information transfer. Phys. Rev. Lett. **85**(2), 461–464 (2000)
42. S.J. Schiff, P. So, T. Chang, R.E. Burke, T. Sauer, Detecting dynamical interdependence and generalized synchrony through mutual prediction in a neural ensemble. Phys. Rev. E **54**, 6708 (1996)
43. D.A. Smirnov, R.G. Andrzejak, Detection of weak directional coupling: Phase-dynamics approach versus state-space approach. Phys. Rev. E **71**(3), 036207 (2005)

44. O. Sporns, R. Kötter, Motifs in brain networks. PLoS Biol. **2**(11), e369 (2004). doi:10.1371/journal.pbio.0020369
45. C. Stam, B.F. Jones, G. Nolte, M. Breakspear, P. Scheltens, Small-world networks and functional connectivity in Alzheimer's disease. Cerebral Cortex **17**, 92 (2007)
46. C. Stam, B. van Dijk, Synchronization likelihood: an unbiased measure of generalized synchronization in multivariate data sets. Physica D **163**, 236 (2002)
47. M. Staniek, K. Lehnertz, Symbolic transfer entropy. Phys. Rev. Lett. **100**(15), 158101 (2008)
48. M. Thiel, M. Romano, J. Kurths, R. Meucci, E. Allaria, F. Arecchi, Influence of observational noise on the recurrence quantification analysis. Physica D **171**, 138–152 (2002)
49. M. Thiel, M.C. Romano, J. Kurths, How much information is contained in a recurrence plot? Phys. Lett. A **330**(5), 343–349 (2004)
50. M. Thiel, M.C. Romano, J. Kurths, M. Rolfs, R. Kliegl, Twin surrogates to test for complex synchronisation. Europhys. Lett. **75**(4), 535 (2006)
51. M. Thiel, M.C. Romano, P.L. Read, J. Kurths, Estimation of dynamical invariants without embedding by recurrence plots. Chaos **14**(2), 234–243 (2004)
52. A.A. Tsonis, K.L. Swanson, Topology and predictability of El Niño and La Niña networks. Phys. Rev. Lett. **100**(22), 228502 (2008)
53. P. Van Leeuwen, D. Geue, M. Thiel, D. Cysarz, S. Lange, M.C. Romano, N. Wessel, J. Kurths, D.H. Grönemeyer, Influence of paced maternal breathing on fetal–maternal heart rate coordination. Proc. Natl. Acad. Sci. USA **106**(33), 13,661–13,666 (2009). doi:10.1073/pnas.0901049106
54. M. Vejmelka, M. Paluš, Inferring the directionality of coupling with conditional mutual information. Phys. Rev. E **77**(2), 026214 (2008)
55. K. Yamasaki, A. Gozolchiani, S. Havlin, Climate networks around the globe are significantly affected by El Niño. Phys. Rev. Lett. **100**(22), 228501 (2008)
56. Y. Zou, M.C. Romano, M. Thiel, N. Marwan, J. Kurths, Inferring indirect coupling by means of recurrences. Int. J. Bifurcation Chaos Appl. Sci. Eng. **21**(04), 1099–1111 (2011). doi:10.1142/S0218127411029033